Morphoarchitectural variation in South African fossil cercopithecoid endocasts

Amélie Beaudet[a, b, *], Jean Dumoncel[b, c], Frikkie de Beer[d], Benjamin Duployer[e], Stanley Durrleman[f], Emmanuel Gilissen[g], Jakobus Hoffman[d], Christophe Tenailleau[e], John Francis Thackeray[h], José Braga[b, h].

[a]*Department of Anatomy, University of Pretoria, PO Box 2034, Pretoria 0001, South Africa*

[b]*Laboratoire d'Anthropologie Moléculaire et Imagerie de Synthèse, UMR 5288 CNRS-Université de Toulouse (Paul Sabatier), 37 Allées Jules Guesde, 31073 Toulouse Cedex 3, France*

[c]*Institut de Recherche en Informatique de Toulouse, UMR 5505 CNRS-Université de Toulouse (Paul Sabatier), 118 Route de Narbonne, 31062 Toulouse Cedex 9, France*

[d]*Radiation Science Department, South African Nuclear Energy Corporation, Pelindaba, North West Province, South Africa*

[e]*Centre Inter-universitaire de Recherche et d'Ingénierie des Matériaux, UMR 5085 CNRS-Université de Toulouse (Paul Sabatier), 118 route de Narbonne, 31062 Toulouse Cedex 9, France*

[f]*Aramis team, INRIA Paris, Sorbonne Universités, UPMC Université Paris 06 UMR S 1127, Inserm U 1127, CNRS UMR 7225, Institut du Cerveau et de la Moelle épinière, 47 boulevard de l'hôpital, 75013 Paris, France*

[g]*Department of African Zoology, Royal Museum for Central Africa, Leuvensesteenweg, 3080 Tervuren, Belgium*

[h]*Evolutionary Studies Institute, University of the Witwatersrand, Private Bag 3, Wits 2050, Johannesburg, South Africa*

Keywords: Endocranial organization; Old World monkey taxonomy; Deformation-based models; Plio-Pleistocene; *Theropithecus; Cercopithecoides*

Abstract

Despite the abundance of well-preserved crania and natural endocasts in the South African Plio-Pleistocene cercopithecoid record, which provide direct information relevant to the evolution of their endocranial characteristics, few studies have attempted to characterize patterns of external brain morphology in this highly successful primate Superfamily. The availability of non-destructive penetrating radiation imaging systems, together with recently developed computer-based analytical tools, allow for high resolution virtual imaging and modelling of the endocranial casts and thus disclose new perspectives in comparative paleoneurology. Here, we use X-ray microtomographic-based 3D virtual imaging and quantitative analyses to investigate the endocranial organization of 14 cercopithecoid specimens from the South African sites of Makapansgat, Sterkfontein, Swartkrans, and Taung. We present the first detailed comparative description of the external neuroanatomies that characterize these Plio-Pleistocene primates. Along with reconstruction of endocranial volumes, we combine a semi-automatic technique for extracting the neocortical sulcal pattern together with a landmark-free surface deformation method to investigate topographic differences in morphostructural organization. Besides providing and comparing for the first time endocranial volume estimates of extinct Plio-Pleistocene South African cercopithecoid taxa, we report additional information regarding the variation in the sulcal pattern of *Theropithecus oswaldi* subspecies, and notably of the central sulcus, and the neuroanatomical condition of the colobine taxon *Cercopithecoides williamsi*, suggested to be similar for some aspects to the papionin pattern, and discuss potential phylogenetic and taxonomic implications. Further research in virtual paleoneurology, applied to specimens from a wider geographic area, is needed to clarify the polarity, intensity, and timing of cortical surface evolution in cercopithecoid lineages.

Introduction

Recent research employing three dimensional (3D) imaging techniques has provided important insights into the brain organization of early cercopithecoids and hence Old World monkeys as a whole (Gonzales et al., 2015). However, relatively little is known about patterns of cercopithecoid brain evolution more generally, despite the extensive Plio-Pleistocene fossil record. The handful of previous studies has focused mainly on one genus, *Theropithecus* (Falk, 1981; Elton et al., 2001), or estimating endocranial volume (ECV; e.g. Martin 1993), although more recent work has highlighted the potential utility of examining the internal morphostructure of Plio-Pleistocene cercopithecoids (Beaudet, 2015; Beaudet et al., 2015, 2016). In part, the lack of attention has been because of a paucity of natural endocasts plus methodological limitations in studying cranial material, notwithstanding its abundance. Fortunately, recent advances in the use of high-resolution 3D imaging and computer-assisted analytical approaches have provided the means with which to examine, in much more detail, cranial material from the extensive Old World monkey fossil record and hence fill important gaps in our knowledge of cercopithecoid brain evolution.

The Plio-Pleistocene cercopithecoid record of South Africa samples at least seven cercopithecoid genera and up to twelve species, with fossil material including several complete skulls and/or nearly intact natural endocasts (Freedman, 1957; Szalay and Delson, 1979; Delson, 1984, 1988; Jablonski, 2002; Gilbert, 2007, 2013; McKee et al., 2011). Three *Parapapio* species are currently recognised in South Africa (*Parapapio broomi*, *Parapapio jonesi*, and *Parapapio whitei*) plus the "*Parapapio*" morph identified at Taung and originally attributed to *Parapapio antiquus* (Freedman, 1957; Szalay and Delson, 1979), along with three extinct variants of *Papio*: *Papio angusticeps, Papio izodi*, and *Papio robinsoni* (Freedman, 1957; Delson, 1984; McKee, 1993; McKee and Keyser, 1994). All the *Parapapio*

taxa (including some material attributed to *Pp. antiquus*) plus *P. izodi* contain specimens for which endocranial morphology can be assessed. *Theropithecus oswaldi* is also found in South Africa, divided into three chronosubspecies (from oldest to youngest): *Theropithecus oswaldi darti*, *Theropithecus oswaldi oswaldi*, and *Theropithecus oswaldi leakeyi* (Leakey, 1993; Frost and Delson, 2002; Frost, 2007). Although Plio-Pleistocene *Theropithecus* brain evolution has been the subject of previous work (Falk, 1981; Elton et al., 2001), sampling the *T. o. darti* material from Makapansgat is particularly relevant as it was not included in Falk's seminal 1981 study of sulcal patterning and its implications for function and evolutionary history. Aspects of endocranial form can also be studied in *T. o. oswaldi* from Swartkrans, but unfortunately not in two further large-bodied papionin taxa, *Dinopithecus ingens* and *Gorgopithecus major*, as they are represented mainly by fragmentary remains (Freedman, 1957; Delson, 1984; Jablonski, 2002; Jablonski and Frost, 2010). The same is true for specimens from Kromdraai, Makapansgat, and Swartkrans that have been assigned to *Cercocebus* sp. (Eisenhart, 1974; Delson, 1984, 1988). However, it is possible to examine *Cercopithecoides williamsi*, one of two extinct colobine species (the other being *Cercopithecoides haasgati*) recognized in the South African Plio-Pleistocene (Delson, 1984, 1988; Jablonski, 2002; McKee et al., 2011), which provides insight into the colobine as well as the cercopithecine radiation. The fossil monkeys from South Africa are therefore an appropriate and suitably diverse group on which new methodological advances can be applied to increase our knowledge of cercopithecoid brain evolution.

Knowledge of primate brain evolution is based both on comparative information from living species whose brains and behavior can be directly investigated (Armstrong and Falk, 1982) and the interpretation of paleoneurological evidence. To date, much of that paleoneurological evidence has come from the study of endocasts. Fossil endocasts consist of replicas of the internal table of the bony braincase and provide the only direct evidence of

brain evolution. When the neurocranium is filled with sediment during fossilization, morphological information about the external brain surface may be preserved as a natural endocast, as illustrated in the South African primate fossil record (Brain, 1981; Holloway et al., 2004). Endocasts constitute a proxy for investigating and quantifying variations in brain size, global brain shape, and neocortical surface morphology, including imprints of cerebral convolutions (i.e., gyri and sulci; Holloway, 1978; Holloway et al., 2004; Falk, 2014; Neubauer, 2014). Given the intimate relationships and patterns of co-variation between brain growth and development and its neurocranial bony container, endocasts are suitable proxies when assessing original brain size and morphological details. Recent comparisons between endocranial organization in the brain and endocranial virtual replicas of primate individuals support the close correspondence between endocranial impressions and cerebral sulci and gyri (e.g., Kobayashi et al., 2014).

Following pioneering research in defining the several levels of evidence that can be collected from endocasts, including gross brain size, delineation of cerebral areas, and major sulcal and gyral identifications (Holloway, 1978), availability of non-destructive penetrating radiation imaging systems, together with recently developed computer-based analytical tools, have allowed for high resolution virtual imaging and modelling of endocranial casts, thus disclosing new perspectives in comparative paleoneurology (Zollikofer and Ponce de León, 1998; Zollikofer, 2002; Gunz et al., 2009; Weber and Bookstein, 2011). Digital data make the quantitative analysis of overall endocranial shape possible, notably through geometric morphometric methods (Bruner et al., 2003, 2009, 2010; Bruner, 2004; Neubauer et al., 2009, 2010; Gunz, 2015) and registration of surfaces from the correspondence of anatomical landmarks (Specht et al., 2007). However, the use of a traditional methodological toolkit based on landmarks, semilandmarks, and curves, even if efficient in compartmentalizing the endocranial cavity, captures little information about the brain itself and its subdivisions. One

potential compromise thus proposed in this study is to combine a detailed analysis of sulcal pattern via automatic detection of the neocortical surface together with the characterization of overall endocranial shape via deformation based-models (Durrleman et al., 2012a, b; Dumoncel et al., 2014; Beaudet, 2015). We also aim to show that the different types of evidence available from endocasts and described by Holloway (1978) can be accessed and assessed reliably for South African fossil cercopithecoid endocrania by means of advanced methods of high-resolution 3D imaging and computer-assisted analytical approaches.

In this paper, along with furthering the development of methods for visualizing and quantifying sulcal pattern and endocranial shape, we report new estimates of ECV (a reliable estimate of actual brain size; Isler et al., 2008) for eight South African cercopithecoid taxa. We also consider the implications of our data on endocranial morphology for improving knowledge of the South African cercopithecoid fossil record, including the taxonomy and evolutionary history of Plio-Pleistocene monkeys, that may be derived from study of sulcal patterns and global shape. We are particularly interested in examining two main issues: (1) variation in sulcal pattern in *Theropithecus*, and (2) the endocranial morphology of *C. williamsi*. Falk (1981) noted distinct features in the sulci of *T. o. oswaldi*, specifically a 'hook-like' configuration of the central sulcus, which was not evident in *T. gelada*, and by extending the sample to South African fossils, we explore variation and divergence in the *Theropithecus* lineage further, which in turn gives clues to the evolutionary history of that highly successful and widespread Plio-Pleistocene radiation. Other work on sulcal patterning (Connolly, 1950; Radinsky, 1974; Falk, 1978) has also highlighted taxon-based gross sulcal patterning, for example discriminating between colobines and cercopithecines. Further examination of possible cercopithecine / colobine distinctions is especially interesting given the presence of *C. williamsi* in the South African Plio-Pleistocene fossil monkey assemblage: despite a typical colobine dental morphology and pollical reduction indicating membership of the extant

African colobine clade (Delson, 1975; Szalay and Delson, 1979; Frost et al., 2015), the locomotor and dietary behavior of *C. williamsi*, along with its large size, is consistent with a terrestrial lifestyle that differs substantially from the arboreal existence observed in its living counterparts (Birchette, 1981; Leakey, 1982; Codron et al., 2005) and in many ways seems quite papionin-like. Quantifying its endocranial morphology thus helps to build a fuller picture of this fascinating animal.

Material and methods

Sample

Our fossil sample includes 14 specimens from four South African Plio-Pleistocene sites (Makapansgat [Member 4], Sterkfontein [Member 4], Swartkrans [Member 1], and Taung; Brain, 1981; Heaton, 2006), detailed in Table 1.

Our comparative sample of extant specimens (n = 46) comprises 11 cercopithecoid genera with both sub-adult and adult individuals (dental age ranging from M3 crown completion to complete emergence and root apical closure; Table 1). Given that the M1 emergence occurs near the time of the cessation of neural growth (Smith, 1991) and that the main cerebral developmental processes (i.e., corticogenesis) are observed in utero or early in the post-natal period in cercopithecine primates (Fukunishi et al. 2006; Malkova et al., 2006; Kashima et al., 2008; Sawada et al., 2009), we assume that the endocasts extracted in our sample are directly comparable.

Scanning protocol and endocast reconstruction

All of the specimens investigated in this study have been detailed by micro-focus X-ray tomography (µCT) using various systems detailed in Table 1, except for one of the *Mandrillus* individuals detailed by cone beam computed tomography (CBCT) with a spatial resolution of 200 µm because of its large dimensions. The isometric voxel size of the reconstructed volumes ranges from 32.7 to 200 µm (Table 1).

The virtual extraction and reconstruction of endocrania were performed through two distinct protocols. In the case of fossil specimens, with the exception of SK 561, the sediments filling the endocranial cavity were digitally separated from the bony remains through semi-automatic threshold-based segmentation via the Avizo v8.0 software (Visualization Sciences Group Inc.). The virtual endocranial volumes were extracted from the representatives of the extant genera and the fossil specimen SK 561 by using the Endex software (Subsol et al., 2010; http://liris.cnrs.fr/gilles.gesquiere/wiki/doku.php?id=endex).

Taphonomic processes and virtual reconstruction

In our fossil sample, six specimens were affected by taphonomic processes and virtually reconstructed (Supplementary Online Material [SOM] Figs. S1–S2 and related comments in SOM Material and methods). On the whole, the observed diagenetic damages were classified into three categories. First, in the neurocrania of STS 565, MP 221, MP 222, and MP 224, part of the cranial vault is missing, creating a significant hole in the endocranial surface (SOM Figs. S1–S2). Based on the morphology of the available bony parts, the non-preserved regions were artificially and automatically closed by digitizing a curve network around the margin of the missing area and by creating a non-uniform rational basis-spline (NURBS) surface that matched the points along the curves through the Rhino v5.0 software (R. McNeel & Associates; Benazzi et al., 2011). The second category concerns the specimen STS 564, which

lacks the left hemisphere (SOM Figs. S1–S2). In order to generate a complete volume, the well preserved right side was mirrored to artificially reconstruct the opposite side (Gunz et al., 2009). Finally, the last category refers to the specimen TP 8, in which a fissure separates the endocranial filling in two distinct parts that were virtually stitched together (SOM Figs S1–S2).

Endocranial volumes

Endocranial volumes (ECV) were assessed in 51 extant and fossil cercopithecoid specimens identified at the species level. Measurements of ECV have been computed from the unsmooth 2D segmentation labels ("Material statistics" module available on Avizo v8.0). For damaged fossils (i.e., STS 564, STS 565, MP 221, MP 222, MP 224), reconstructed surfaces were used in analysis (SOM Figs S1–S2). Given the allometric relationship between ECV and body mass in primates (Isler et al., 2008), logged (base 10) ECV values were plotted against logged (base 10) body mass estimates, with body mass estimates derived from Smith and Jungers (1997), Delson et al. (2000), and Scott (2011). We consider our ECV analyses to be exploratory and preliminary since aspects such as phylogenetic regression and allometry will not be discussed here.

Deformation-based models

To compare endocranial morphology between species, we used a landmark-free method that relies on the calculation of group-average surface models and their deformation onto the investigated surfaces (Durrleman et al., 2012a, b; Dumoncel et al., 2014, 2016; Beaudet, 2015). The deformation-based models differ substantially from geometric

morphometrics methods because (i) they are not based on prior definition of homologous points but on correspondences between continuous surfaces and (ii) statistics are not performed on the positions of individual points but on deformations (see Durrleman et al., 2012a for further details). Examining deformations between surfaces, mathematically modeled as a "diffeomorphism," is particularly appropriate for comparing overall shapes and local orientation in the field of computational anatomy (Glaunès and Joshi, 2006; Durrleman et al., 2014).

The overall process includes several successive computational steps, illustrated in Figure 1. As a pre-processing step, the surfaces were rigidly aligned in position, orientation, and scale with respect to a reference surface (randomly selected) using the iterative closest point (ICP) algorithm (Fig. 1A). Second, a shape model, called global mean shape (GMS), is computed from the set of aligned surfaces. The construction is done using an iterative optimization algorithm described in Durrleman (2010), which uses an ellipsoid surface as input (Fig. 1B) and yields the GMS as output (Fig. 1C). The algorithm also yields deformation fields, which are the parameters of non-linear deformations registering the GMS to each specimen. They are distributed in a 3D grid enclosing the surfaces and common to all the registrations procedures between the GMS and the specimens (see Durrleman, 2010 for further technical details; Fig. 1C). In our analyses, because the fossil specimens may be taphonomically deformed, GMS was estimated using the extant specimens only. Additionally, based on the results provided by the third step, a taxon mean shape (TMS) was computed for each extant taxon represented in our sample (Fig. 1D). Finally, the Plio-Pleistocene specimens were included in the analysis and the GMS was deformed to each individual (Fig. 1E).

Based on the deformation framework, we generated (i) a GMS associated with a set of deformations from the GMS to each endocranium (hereinafter called "GMS-to-individuals") computed from our extant sample, (ii) a TMS for each extant genus investigated in our study

and represented by more than two individuals, and (iii) deformations from the GMS to fossil endocasts. In addition to GMS-to-individuals deformations, the GMS was also deformed to the TMS (hereinafter called “GMS-to-TMS”).

The magnitude of the displacements recorded during the deformation process (i.e., GMS-to-individuals and GMS-to-TMS) were rendered by color maps from dark blue (lowest displacement values) to red (highest displacement values) on the endocast surfaces (i.e., TMS and individual endocasts; Fig. 1E). In combination with the cartographies, the directions and magnitudes of the deformations from the GMS to the TMS/individuals are represented by vectors (Fig. 1E).

Semi-automatic sulci detection

Some cortical details, including the sulcal imprints, were evident in most of the fossil specimens (SOM Figs. S1–S2). Sulcal pattern is usually identified and described by visual inspection of the endocranial surface. Based on previous studies (Subsol, 1995, 1998), we here use an automatic method for the identification of neocortical relief in endocasts that includes the algorithm presented by Yoshizawa et al. (2007, 2008) for the detection of topographical variations (i.e., crest lines) in 3D meshes. The sulci are considered to be variation points of the surface on a triangle mesh and detected via a geometry-based method using curvature lines computed on the surface. More precisely, the crest lines are defined as salient subsets of the extrema of the principal curvatures on surfaces. The detected structures were corrected manually by removing the non-anatomical features (e.g., cracks due to taphonomic damage), using "The Primate Brain Bank" (www.primatebrainbank.org) and published studies of cercopithecoid endocasts as references (e.g., Connolly, 1950; Falk, 1978,

1981). This "cleaning" step was performed using a program created with MATLAB R2013a v8.1 (Mathworks) by one of us (J.D.).

Multivariate analyses

The deformation fields integrating local orientation and the amplitude of the deformations from the GMS to each specimen (i.e., GMS-to-individuals) were statistically analyzed by computing a between-group principal component analysis (bgPCA; Durrleman, 2010; Mitteroecker and Bookstein, 2011). Based on the covariance matrix of the predefined extant group means, the fossil specimens were subsequently projected into the shape space. Shape changes and morphological trends observed in the specimens/clusters plotted were depicted by color maps and vectors.

A hierarchical clustering on principal components (HCPC) tree, integrating all the bgPCA components, was generated using the FactoMineR package (Lê et al., 2008) for R v.3.2.1 (R Development Core Team, 2015).

Results

Endocranial volumes

The endocranial volumes measured for both extant and fossil cercopithecoid specimens are presented in Table 2 and plotted against body mass in Figure 2. Of these species, *Chlorocebus*, *Erythrocebus,* and *Cercopithecus* have the smallest ECVs relative to body mass. Taking their "medium" body masses into account, the mangabeys *Cercocebus* and *Lophocebus* have relatively larger endocranial capacities than do the colobines *Colobus* and *Piliocolobus*. Most of the living papionins plot on the upper range of the ECV estimates, with

Papio having the largest ECV relative to body mass. On the contrary, the *Macaca* individuals are distributed toward the lower estimates of the papionin cluster. All the fossil specimens fall within or close to the lower limit of extant papionin variation, even *C. williamsi*, which lies closer to extinct *Theropithecus* than to extant colobines.

Morphoarchitectural variation

The bgPCA analysis of endocast deformations is shown in Figure 3 and the color maps illustrating the changes from the GMS to each TMS of extant and fossil individuals are depicted in Figures 4-5 and SOM Figure S3. On the whole, three main groups are evident based on the distribution of the living specimens in shape space, corresponding to the three cercopithecoid tribes (Cercopithecini, Papionini and Colobini) represented in our study (Fig. 3, see also comments SOM Results). Along the second component bgPC2, the extant representatives of the cercopithecin genera *Cercopithecus*, *Chlorocebus*, and *Erythrocebus* are grouped together in the negative values and are clearly separated from the rest of the sample. The extant papionins are grouped in the positive values of both axes. The colobines *Colobus* and *Piliocolobus* are found in the positive space of bgPC2 and negative values of bgPC1.

The fossil papionins plot between the colobines and *Mandrillus* / *Papio*, close to *Macaca* and the mangabeys (Fig. 3). The fossil specimens attributed to *Parapapio* and *Papio* are roughly characterized by an elongation and a relative elevation of the frontal pole compared to the GMS (Fig. 4). The occipital lobes are shifted inferiorly and their volumes are significantly reduced in comparison to the GMS. The endocranial regions affected by taphonomic processes and virtually corrected in STS 565, MP 221, and MP 224 do not contribute to excessive local deformations. The large vector identified in the inferior part of the TP 7 endocast could be related to the manual segmentation performed for the extraction of

the surface. The condition displayed by the taxonomically undetermined specimen STS 538 is close to the *Parapapio* and *Papio* specimens, notably by the elevation of the superior surface and the lower position of the occipital lobes.

The *T*. *o*. *oswaldi* specimen SK 561 is relatively close to the extant representatives of this genus in the bgPCA (Fig. 3). These affinities are explained by the elevation of the superior parietal surface and by the reduction of the temporal lobes (Fig. 5 and SOM Fig. S3). However, the vectors oriented inferiorly, strongly marked, suggest potential diagenetic disorders affecting the surface in contact with the basicranium. The two *T*. *o*. *darti* specimens, M 3073 and MP 222, group more closely with fossil *Parapapio* and *Papio* and with the *Macaca* and *Lophocebus* conditions than to extant *Theropithecus* in shape space. The color maps point out a significant contraction of the parietal superior surface for MP 222, corresponding to the reconstructed region and responsible for the relative elevation of the occipital and frontal lobes. The M 3073 specimen is close to the GMS and differs from the reference mainly by a bi-temporal enlargement.

The deformation pattern displayed by the fossil specimen M 3055, attributed to *C*. *williamsi* and included in extant colobine variability in the bgPCA, is shared with extant colobines (Fig. 5 and SOM Fig. S3). On the contrary, the two other *C*. *williamsi* specimens, MP 36 and MP 3a, are closer to the fossil papionins than to the extant colobines. MP 3a shares temporal lobe reduction with living colobines as illustrated by the vectors oriented ventro-dorsally (Fig. 5 and SOM Fig. S3), although it also has substantial contraction of the left occipital lobe.

The HCPC computed on the results of the deformation process is shown in Figure 6. As for the bgPCA, our sample is roughly divided into three main clusters corresponding to the tribes Papionini, Colobini, and Cercopithecini. Among the Papionini, the extant representatives of *Papio* (Fig. 6, group G) and *Mandrillus* (Fig. 6, group F) are clearly separated from the other

members of the tribe, in accordance with the specific morphology depicted by the color maps and the vectors (SOM Fig. S3). The affinities of SK 561 with extant *Theropithecus* are supported by its inclusion among the geladas, and so is the relationship between M 3055 and the extant colobines. As previously mentioned, MP 222 is close to *Macaca*, but the influence of the reconstructed cranial vault needs to be clarified. Interestingly, the majority of the fossil specimens are included in groups D and E of Figure 6, which separate the specimens of Makapansgat from the specimens of Sterkfontein and Taung, independent of individual taxonomic affiliation. The Makapansgat group also includes the *Lophocebus* specimens. According to the deformation maps (Figs. 4–5 and SOM Fig. S3), the shift of the occipital lobes to an inferior position is combined with an elongation of the frontal pole for the Makapansgat specimens, contributing to a relatively straighter overall profile than the Sterkfontein and Taung specimens, which are more globular.

Sulcal pattern

The extant cercopithecoid sulcal condition, including members of the cercopithecin, papionin, and colobinan tribes, is represented by selected specimens in SOM Figures S4–S5 and described in related comments (SOM Results). In summary, the basic cercopithecine sulcal pattern that we observed in this sample corresponds to the previous descriptions of Connolly (1950) and Falk (1978). One of the most critical neocortical features that helps discriminate the colobine brain (both African and Asian) from the cercopithecine cerebral condition is the presence of paroccipital sulcus (Falk, 1978). Unfortunately, because of relatively faint sulcal imprints in the parietal and occipital regions of endocasts, we were not able to detect this critical structure in our endocasts.

Results of the automatic detection of neocortical sulci in the fossil sample are illustrated in Figures 7–8 for *Papio*, *Parapapio*, *Theropithecus*, and *Cercopithecoides*. Globally, *Parapapio* and fossil *Papio* from Makapansgat, Taung, and Sterkfontein exhibit the extant papionin sulcal pattern (Fig. 7 and SOM Fig. S4). The frontal fissures are composed of a V-shape arcuate sulcus and a principal sulcus that diverges from the orbital margin. The subcentral anterior sulcus is potentially identified in STS 564, as well as in MP 221 and MP 3133, and is close to the arcuate sulcus. The presence of the subcentral posterior sulcus is suggested for M 3133 based on its posterior position in relation to the inferior part of the central sulcus. The inferior extremities of the central and the intraparietal sulci are curved caudally and rostrally, respectively, as also seen in extant papionins (Fig. 7 and SOM Fig. S4). The inferior occipital sulcus is found in all fossil *Papio* and *Parapapio* specimens with the exception of MP 224 and TP8. The lateral sulcus systematically intercepts the superior temporal sulcus except in the left hemisphere of MP 221. Finally, the overall fissure pattern observed in the taxonomically undetermined specimen STS 538 is close to the *Parapapio* condition.

While the principal sulcus position in *T*. *o*. *darti* is close to the papionin pattern (Fig. 8), the arcuate sulcus is relatively curved, as in colobines (SOM Fig. S5). The subcentral anterior sulcus is identified on the right hemisphere of M 3073 and is connected to the arcuate sulcus. The subcentral posterior sulcus on the left hemisphere of M 3073 is linked with the central sulcus, whereas the central sulcus curves sharply in a caudal direction in the right hemisphere (‘hook-like’ configuration). The intraparietal and lunate sulci are relatively straight and the inferior occipital sulcus is identified only on the left hemisphere in the case of M 3073.

For *C*. *williamsi*, except in the left hemisphere of M 3055, the lateral and temporal superior sulci converge but do not intercept, in a similar fashion to *Colobus*. The frontal sulcal pattern in *C*. *williamsi* specimens MP 3a and MP 36 is similar to that of the extant papionins, based on the presence of relatively straight grooves and the divergence of the principal sulcus from

the orbital margin, whereas the configuration in M 3055 is colobine-like (Fig. 8). The position of the subcentral anterior sulcus in the right hemispheres of MP 36 and M 3055 is similar to that described for *Colobus* (SOM Fig. S5), but also to fossil papionins (Fig. 7). In all three specimens investigated, the inferior end of the central sulcus is curved, as in contemporaneous fossil papionin specimens. The configuration of the central sulcus in MP 36 differs from the two other specimens, having a very short cleft connected inferiorly, which could potentially be identified as the sulcus subcentralis posterior, contributing to an overall curved aspect. This sulcal arrangement nears the one detected in *T. o. darti* in our study.

Discussion

Endocranial volumes

To the best of our knowledge, this current study reports and compares for the first time the ECVs of Plio-Pleistocene South African cercopithecoid taxa, with the exception of extinct *Theropithecus*, for which ECVs were previously estimated by Martin (1993) and Elton et al. (2001). Our estimates of *T. oswaldi* ECVs (134–170 cm^3, including both *T. o. oswaldi* and *T. o. darti*) fit within the fairly wide range estimated by Martin (1993; 154–200 cm^3) from three *T. oswaldi* crania from East Africa (Peninj DAT 600/82, a *T. oswaldi* female, Kanjera BM 32102, a *T. oswaldi* male, and Kanjera BM 14936, a *T. oswaldi* female). In contrast, ECVs of *T. o. oswaldi* (168 cm^3 for SK 561) and *T. o. darti* (134 cm^3 for MP 222 and 170 cm^3 for M 3073) reported in our study are higher than the Elton et al. (2001) estimates (150 cm^3 for *T. o. oswaldi* SK 561, 122 cm^3 for *T. o. darti* MP 222, and 143 cm^3 for M 3073; based on regression equations assessed specifically on *Theropithecus*). The differences between our and previous studies might be explained by the methods used performed, as we estimate

ECVs directly by virtually filling the neurocranium and extracting the endocranial volume rather than packing the braincase with seeds (Martin, 1993) or using regression equations derived from the relationship between external cranial dimensions and whole cranial capacity in extant *Theropithecus* and cercopithecoids (Elton et al., 2001). Besides being noninvasive, the assessment of ECVs based on high-resolution imaging techniques and virtual reconstruction of endocasts is important for understanding primate paleoneurology, not only because of the more direct means of ECV estimation but also because ECV can be more reliably delimited through the virtual exploration of internal bony structures. In addition, our techniques allow the inclusion of incomplete skulls (e.g., MP 222).

Our current study is focused primarily on methodological development, and hence presents preliminary results. It will need to be extended considerably in the future by integrating a larger sample of extant and fossil cercopithecoids (e.g., a total of 339 and 22 extant and fossil cercopithecoid specimens respectively were sampled in Elton et al. [2001]) and considering and testing crucial variables such as sexual dimorphism and allometry. This notwithstanding, in our study, extant *Papio* has the largest ECVs relative to body size among both extant and extinct cercopithecoid taxa considered, as is also true for brain weight (Martin, 1993). *Macaca* specimens (particularly *Macaca mulatta*) had some of the lowest ECV values for cercopithecoids of 'medium' body mass. A similar finding has previously been reported for *Macaca sylvanus* (Isler et al., 2008) but, as in the present study, interpretation was hindered by the small sample. The ECVs computed in our study also conform to previous work showing that extant colobines have smaller brains than other cercopithecoids (Martin, 1993; Isler et al., 2008). One of the most interesting results in our study concerned ECV in the fossil colobine *C. williamsi*, which grouped with the fossil cercopithecine specimens, and at the upper end of the extant cercopithecoid range. At ~20 kg (Delson et al., 2000), *C. williamsi* was much larger than extant African colobines, so it is

difficult to make direct comparisons with its closest modern relatives without a full allometric analysis. Nonetheless, smaller brains (as seen in extant African colobines) may be related to folivory (Martin, 1993), so the fact that *C*. *williamsi*, probably a terrestrial forager (Codron et al., 2005), groups with the other large Plio-Pleistocene cercopithecoids lends support to arguments that it was adaptively different to modern African colobines. It would be informative to investigate the ECVs of terrestrial Plio-Pleistocene East African *Cercopithecoides* taxa estimated to be smaller (C. *alemayehui*, *C*. *kerioensis*, *C*. *meaveae*) or bigger (*C*. *kimeui*) than *C*. *williamsi* (Jablonski and Frost, 2010).

Taxonomic and evolutionary implications of endocranial organization

In general, the sulcal patterns we observed in the present study conformed to those previously described for cercopithecines (Connolly, 1950; Falk, 1978). In *Parapapio*, the organization of the parietal sulci, and especially the position of the central and intraparietal sulci, is consistent across individuals. The taxonomically undetermined specimen STS 538 shares features with the specimens identified as *Parapapio*, consistent with previous tentative assignment based on external cranial morphology (Heaton, 2006). The distinction between the gross endocranial morphology of cercopithecoid specimens from Makapansgat Member 4, on the one hand, from the slightly younger Taung and Sterkfontein Member 4 assemblages, on the other hand, needs to be explained by further investigations of the fossil record, testing potential temporal sensitivity of endocranial organization (Delson, 1984, 1988; McKee, 1993; McKee et al., 1995).

Our visualizations also highlighted interesting variation that adds to our knowledge of sulcal pattern in Old World monkeys. In the *T*. *o*. *darti* specimen M 3073, the subcentral posterior sulcus in the left hemisphere, linked with the central sulcus, appears similar to those

described for *T*. *o*. *oswaldi* L 238-29 from Omo (Falk, 1981). Comparing *T*. *o*. *darti* M 3073 with the other Makapansgat *T*. *o*. *darti*, MP 222 (neither of which were available for study by Falk [1981]), as well as the forms from Hadar described by Falk (1981), it is evident that considerable variation exists within the subspecies. This variation might overlap with that observed in previous work (Falk, 1981) on eastern African *T*. *o*. *oswaldi*.

Falk (1981) suggested that the strongly curved ('hook-like') inferior end of the central sulcus resulted from the merging of the central and subcentral posterior sulci and is derived for *T*. *o*. *oswaldi* compared to *T*. *o*. *darti*. We suggest that *T*. *o*. *darti* from Makapansgat may show a transitional gyrification pattern, which could stretch the appearance of the derived condition back to c. 3 Ma (Brock et al., 1977; McFadden et al., 1979; Delson, 1984), rather than to 1.9–2.0 Ma as initially proposed by Falk (1981). Moreover, the 'hook-like' configuration is not found among extant geladas, where the subcentral posterior sulcus remains perceptible. Accordingly, based on this potential autapomorphic feature, the divergence of the extant *Theropithecus gelada* lineage from the *T*. *oswaldi* lineage could predate the chronological period represented by Makapansgat Member 4, as proposed by Jolly (1972). However, given that the mechanism for the formation of folding in the primate cortex is not yet fully understood (even if probably related to biomechanical constraints [Van Essen, 1997; Hilgetag and Barbas, 2005; Toro and Burnod, 2005; Toro, 2012; Bayly et al., 2014; Tallinen, 2016]), phylogenetic interpretations of sulcal pattern should be considered tentative. It is acknowledged that genetic factors are known to influence the developmental pattern and mechanical forces acting on cortical sheet expansion and folding (Rakic, 1995; Bae et al., 2014). It is thus possible that allometric factors influence gyral and sulcal pattern in *Theropithecus*. This has implications for the way in which we interpret the evolutionary relevance of sulcal pattern, particularly since a correlation has been reported between increase in brain size and increase in gyrencephaly in mammal orders (Pillay and Manger, 2007).

Moreover, because of the mechanisms of gyrogenesis (Welker, 1990), variation in developmental process may also contribute to sulcal patterns in mature individuals. Accordingly, cerebral ontogenetic changes may also play a role in the variation seen in the genus *Theropithecus*, especially given the developmental differences described for extant geladas compared to other papionins (Swindler and Beynon, 1993).

Another intriguing finding was the variation we observed in *C*. *williamsi* endocranial organization. All three specimens included in this study that are assigned to *C*. *williamsi* shared features with *Colobus*, as revealed by the statistical classification of the well-preserved specimen M 3055 among extant colobines, although the morphoarchitecture of *C*. *williamsi* endocasts does not mirror the pattern seen in extant colobines: specific colobine-like structures such as the paroccipital sulcus were not identified in our *Cercopithecoides* sample, even if as pointed out by Tobias (1987: 746) "valuable information may flow from the presence of a sulcus or of a convolutional bulge on an endocast, whereas the absence of an impression may be of dubious morphological significance". One specimen, MP 36, also showed a configuration of the inferior part of the central sulcus very similar to the *T*. *o*. *darti* specimen M 3073. MP 36 is mainly represented by the neurocranium and meager tooth fragments, and has variously been attributed to *Simopithecus darti* (by R. Broom and J.S. Jensen; see Freedman [1957]), *Pp*. *broomi* (Freedman, 1957; Eisenhart, 1974), and, most recently, *C*. *williamsi* (Fourie et al., 2008). Given the sulcal similarities we observed between MP 36 and M 3073, it is possible that MP 36 is actually *T*. *o*. *darti*, although more research to illuminate species-specific variation in cercopithecoids would be desirable. Additional research would also be useful to help understand the evolutionary history of sulcal pattern in colobines. The extant colobine sulcal pattern as described by Falk (1981) in African and Asian taxa, characterized notably by the presence of an arched intraparietal sulcus and the divergence of the principal sulcus from the orbital border, among other aspects, is present in

Mesopithecus pentelici (Radinsky, 1974), a Eurasian Pliocene colobine. Recent work has suggested that *Cercopithecoides williamsi* is a definitive member of the African colobine clade (Frost et al., 2015), implying that modern African colobines are more distantly related to *Mesopithecus* than they are to *C. williamsi*. Thus, similarities in the sulcal patterns of *Mesopithecus* and extant African colobines must either have arisen convergently, or *Cercopithecoides* shows sulcal morphology that is derived relative to other colobines. Our knowledge of this would also be enhanced further by including *Cercopithecoides haasgati* (McKee et al., 2011), and indeed other large African colobines, into analyses.

It must also be considered that sulcal pattern may be linked to function, and it is possible that functional convergence may explain some of the similarities between *C. williamsi* and papionins. Based on sulcal pattern, Falk (1981) hypothesized that *T. oswaldi* had a relatively expanded cortical somatic sensory and motor face representation compared to the geladas, potentially due to the specialization for mastication of abrasive food. However, making interpretations of function from sulcal pattern is problematic: some inconsistencies in correspondence between sulcal and cytoarchitectural areas have been identified, meaning that the cerebral areas delimitated by sulci on the external cortical surface do not systematically coincide with functional areas (Amunts et al., 1999; but see Fischl et al., 2008). Hence, very little can be reasonably inferred about function from our data.

Conclusions

Despite the relative abundance of nearly complete cercopithecoid neurocrania in the paleontological assemblages, endocranial condition has not yet been fully detailed in the South African Plio-Pleistocene records, mainly because of the difficulties related to the extraction of fossil endocasts. Through non-destructive X-ray radiation based high-resolution

3D tomography imaging techniques, we successfully reconstructed virtual endocrania from a representative sample of fossil cercopithecoids and reported ECVs for the first time, as well as morphological and structural variations. In particular, we contributed more information regarding the variation in sulcal pattern in *Theropithecus*. As previously suggested in the East African context, the *Theropithecus* fossil lineages present specific derived sulcal patterns, suggested to be useful for taxonomic identification, especially of isolated neurocrania. The identification of this landmark feature in the Makapansgat record supports the possibility of the divergence between the *Theropithecus* fossil lineages and *Theropithecus gelada* prior to 3 Ma. Our investigation of *C. williamsi* endocasts reveals an ECV and sulcal pattern similar to the papionin condition. Given that *Cercopithecoides*, a committed terrestrialist, differed substantially from the arboreal existence observed in its living counterparts, similarities with papionins in terms of cortical organization might potentially support the hypothesis of an extinct colobine taxon that was adaptively different to modern African colobines.

Besides traditional analyses of the outer cranial morphology, high resolution virtual imaging of fossil primate endocasts allowing the automatic detection of neocortical relief coupled with deformation-based models and morphometrical analyses have the potential to add a significant amount of taxonomic and phylogenetic information. Further research in virtual endocranial paleoprimatology to be developed at a continental scale, including fossil specimens from the rich East African cercopithecoid-bearing sites and notably representatives of the *Theropithecus* genus (Jablonski, 1993; Frost, 2001, 2007; Frost and Delson, 2002; Frost and Alemseged, 2007; Jablonski and Leakey, 2008; Gilbert et al., 2011; Frost et al., 2014), would better clarify the polarity, intensity, and timing of the evolutionary changes among cercopithecoid lineages.

Acknowledgments

We are indebted to S. Potze (Pretoria), B. Zipfel (Johannesburg), J. Cuisin (Paris), G. Fleury (Toulouse), and W. Wendelen (Tervuren) for having granted access to fossil and comparative material under their care. We also thank K. Carlson and T. Jashashvili (Johannesburg), G. Clément and M. Garcia-Sanz (Paris), L. Bam (Pretoria), and D. Maret and E. Coudrais (Toulouse) for (micro-X-ray) tomographic and CBCT acquisitions, and E. Delson (New York) for providing CT scans. For scientific contribution and/or for discussion and comments to the results presented in this study, we are especially grateful to E. Delson (New York), D. Ginibriere (Toulouse), J. Heaton (Birmingham), N. Jablonski (University Park), O. Kullmer (Frankfurt), R. Macchiarelli (Poitiers & Paris), M. Nakatsukasa (Kyoto), L. Pan (Toulouse), and C. Zanolli (Toulouse). The present version greatly benefited from the comments provided by the Editor, the Associate Editor, and three anonymous reviewers. The French research federation FERMaT (FR3089), the National Research Foundation (NRF), and Department of Science and Technology (DST) of South Africa are acknowledged for providing micro-X-ray tomography laboratory facilities. This work was granted access to the HPC resources of CALMIP supercomputing center under the allocation 2015-[P1440] attributed to the AMIS laboratory. Research supported by the Center of Research and Higher Education (PRES) of Toulouse, the Midi-Pyrénées Region, and the French Ministry of Foreign Affairs.

References

Amunts, K., Schleicher, A., Bürgel, U., Mohlberg, H., Uylings, H. B.M., Zilles, K., 1999. Broca's region revisited: cytoarchitecture and intersubject variability. J. Comp. Neurol., 412, 319–341.

Armstrong, E., Falk, D., 1982. Primate Brain Evolution. Methods and Concepts. Plenum Press, New York.

Bae, B.-I., Tietjen, I., Atabay, K.D., Evrony, G.D., Johnson, M.B., Asare, E., Wang, P.P., Murayama, A.Y., Im, K., Lisgo, S.N., Overman, L., Sestan, N., Chang, B.S., Barkovich, A.J., Grant, P.E., Topcu, M., Politsky, J., Okano, H., Piao, X., Walsh, C.A., 2014. Evolutionarily dynamic alternative splicing of GPR56 regulates regional cerebral cortical patterning**.** Science 343, 764–768.

Bayly, P., Taber, L., Kroenke, C., 2014. Mechanical forces in cerebral cortical folding: a review of measurements and models. J. Mech. Behav. Biomed. Mater. 29, 568–581.

Beaudet, A., 2015. Caractérisation des structures crânio-dentaires internes des cercopithécoïdes et étude diachronique de leurs variations morphologiques dans la séquence Plio-Pléistocène sud-africaine. Ph.D. Dissertation, Université de Toulouse.

Beaudet, A., Zanolli, C., Engda Redae, B., Endalamaw, M., Braga, J., Macchiarelli, R., 2015. A new cercopithecoid dentognathic specimen attributed to *Theropithecus* from the late Early Pleistocene (c. 1 Ma) deposits of Simbiro, at Melka Kunture, Ethiopian highlands. Palevol. 14, 657–669.

Beaudet, A., Braga, J., de Beer, F., Schillinger, B., Steininger, C., Vodopivec, V., Zanolli, C., 2016. Neutron microtomography-based virtual extraction and analysis of a cercopithecoid partial cranium (STS 1039) embedded in a breccia fragment from Sterkfontein Member 4 (South Africa). Am. J. Phys. Anthropol. 159, 737–745.

Benazzi, S., Bookstein, F.L., Strait, D.S., Weber, G.W., 2011. A new OH5 reconstruction with an assessment of its uncertainty. J. Hum. Evol. 61, 75–88.

Birchette, M.G., 1981. Postcranial remains of *Cercopithecoides*. Am. J. Phys. Anthropol. 54, 201.

Brain, C.K., 1981. The Hunters of the Hunted? An introduction to African Cave Taphonomy. University of Chicago Press, Chicago.

Brock, A., McFadden, P.L., Partridge, T.C., 1977. Preliminary paleomagnetic results from Makapansgat and Swartkrans. Nature 266, 249–250.

Bruner, E., 2004. Geometric morphometrics and paleoneurology: brain shape evolution in the genus *Homo*. J. Hum. Evol. 47, 279–303.

Bruner, E., Manzi, G., Arsuaga, J.L., 2003. Encephalization and allometric trajectories in the genus *Homo*: evidence from the Neandertal and modern lineages. Proc. Natl. Acad. Sci. U.S.A. 100, 15335–15340.

Bruner, E., Mantini, S., Ripani, M., 2009. Landmark-based analysis of the morphological relationship between endocranial shape and traces of the middle meningeal vessels. Anat. Rec. 292, 518–527.

Bruner, E., Martin-Loeches, M., Colom, R., 2010. Human midsagittal brain shape variation: patterns, allometry and integration. J. Anat. 216, 589–599.

Codron, D., Luyt, J., Lee-Thorp, J., Sponheimer, M., deRuiter, D., Codron, J., 2005. Utilization of savanna-based resources by baboons during the Plio-Pleistocene. S. Afr. J. Sci. 10, 245–248.

Connolly, C.J., 1950. External Morphology of the Primate Brain. C.C. Thomas, Springfield.

Delson, E., 1975. Evolutionary history of the Cercopithecidae. In: Szalay, F.S. (Ed.), Approaches to Primate Paleobiology. Contributions to Primatology 4, Karger, Basel, pp. 167–217.

Delson, E., 1984. Cercopithecoid biochronology of the African Plio-Pleistocene: correlation among eastern and southern hominid-bearing localities. Cour. Forsch. Inst. Senckenberg 69, 199–281.

Delson, E., 1988. Chronology of South African australopiths site units. In: Grine, F.E. (Ed.), Evolutionary History of the 'Robust' Australopithecines. Aldine de Gruyter, New York, pp. 317–324.

Delson, E., Terranova, C.J., Jungers, W.L., Sargis, E.J., Jablonski, N.G., Dechow, P.C., 2000. Body mass in Cercopithecidae (Primates, Mammalia): estimation and scaling in extinct and extant taxa. Anthropol. Pap. Am. Mus. Nat. Hist. Vol. 83. 1-159.

Dumoncel, J., Durrleman, S., Braga, J., Jessel, J.-P., Subsol G., 2014. Landmark-free 3D method for comparison of fossil hominins and hominids based on endocranium and EDJ shapes. Am. J. Phys. Anthropol. 153 (Suppl. 56), 110.

Dumoncel, J., Subsol, G., Durrleman, S., Jessel, J.-P., Beaudet, A., Braga, J., 2016. How to Build an Average Model When Samples Are Variably Incomplete? Application to Fossil Data. The IEEE Conference on Computer Vision and Pattern Recognition (CVPR) Workshops, pp. 101-108.

Durrleman, S., 2010. Statistical Models of Currents for Measuring the Variability of Anatomical Curves, Surfaces and their Evolution. Ph.D. Dissertation, Université Nice-Sophia Antipolis.

Durrleman, S., Pennec, X., Trouvé, A., Ayache, N., Braga, J., 2012a. Comparison of the endocranial ontogenies between chimpanzees and bonobos via temporal regression and spatiotemporal registration. J. Hum. Evol. 62, 74–88.

Durrleman, S., Prastawa, M., Korenberg, J.R., Joshi, S., Trouvé, A., Gerig, G., 2012b. Topology preserving atlas construction from shape data without correspondence using

sparse parameters. In: Ayache, N., Delingette, H., Golland, P., Mori, K. (Eds.), MICCAI 2012, Part III. LNCS, vol. 7512. Springer, Heidelberg, pp. 223–230.

Durrleman, S., Prastawa, M., Charon, N., Korenberg, J.R., Joshi, S., Gerig, G., Trouvé, A., 2014. Morphometry of anatomical shape complexes with dense deformations and sparseparameters. NeuroImage 101, 35–49.

Eisenhart, W.L., 1974. The fossil cercopithecoids of Makapansgat and Sterkfontein. A.B. Thesis, Harvard College.

Elton, S., Bishop, L.C., Wood, B., 2001. Comparative context of Plio-Pleistocene hominin brain evolution. J. Hum. Evol. 41, 1–27.

Falk, D., 1978. Brain evolution in Old World Monkeys. Am. J. Phys. Anthropol. 48, 315–320.

Falk, D., 1981. Sulcal patterns of fossil *Theropithecus* baboons: phylogenetic and functional implications. Int. J. Primatol. 2, 57–69.

Falk, D., 2014. Interpreting sulci on hominin endocasts: old hypotheses and new findings. Front. Hum. Neurosci. 8, 134.

Fischl, B., Rajendran, N., Busa, E., Augustinack, J., Hinds, O., Yeo, B.T., Mohlberg, H., Amunts, K., Zilles, K., 2008. Cortical folding patterns and predicting cytoarchitecture. Cereb. Cortex 18, 1973–1980.

Fourie, N.H., Lee-Thorp, J.A., Ackermann, R.R., 2008. Biogeochemical and craniometric investigation of dietary ecology, niche separation, and taxonomy of Plio-Pleistocene cercopithecoids from the Makapansgat Limeworks. Am. J. Phys. Anthropol. 135, 121–135.

Freedman, L., 1957. The fossil Cercopithecoidea of South Africa. Ann. Transv. Mus. 23, 121–262.

Freedman, L., 1961. New cercopithecoid fossils, including a new species, from Taung, Cape Province, South Africa. Ann. S. Afr. Mus. 46, 1–14.

Freedman, L., 1976. South African fossil Cercopithecoidea: a re-assessment including a description of new material from Makapansgat, Sterkfontein and Taung. J. Hum. Evol. 5, 297–315.

Frost, S.R., 2001. Fossil Cercopithecidae of the Afar Depression, Ethiopia: species systematics and comparison to the Turkana Basin. Ph.D. Dissertation, The City University of New York.

Frost, S.R., 2007. Fossil Cercopithecidae from the Middle Pleistocene Dawaitoli Formation, Middle Awash Valley, Afar Region, Ethiopia. Am. J. Phys. Anthropol. 134, 460–471.

Frost, S.R., Alemseged, Z., 2007. Middle Pleistocene fossil Cercopithecidae from Asbole, Afar Region, Ethiopia. J. Hum. Evol. 53, 227–259.

Frost, S.R., Delson, E., 2002. Fossil Cercopithecidae from the Hadar Formation and surrounding areas of the Afar Depression, Ethiopia. J. Hum. Evol. 43, 687–748.

Frost, S.R., Jablonski, N.G., Haile-Selassie, Y., 2014. Early Pliocene Cercopithecidae from Woranso-Mille (Central Afar, Ethiopia) and the origins of the *Theropithecus oswaldi* lineage. J. Hum. Evol. 76, 39–53.

Frost, S.R., Gilbert, C.C., Pugh, K.D., Guthrie, E.H., Delson, E., 2015. The hand of *Cercopithecoides williamsi* (Mammalia, Primates): earliest evidence for thumb reduction among colobine monkeys. PLoS ONE 10(5), e0125030. doi:10.1371/journal.pone.0125030.

Fukunishi, K., Sawada, K., Kashima, M., Sakata-Haga, H., Fukuzaki, K., Fukui, Y., 2006. Development of cerebral sulci and gyri in fetuses of cynomolgus monkeys (*Macaca fascicularis*). Anat. Embryol. (Berl.) 211, 757–764.

Gilbert, C.C., 2007. Craniomandibular morphology supporting the diphyletic origin of mangabeys and a new genus of the *Cercocebus*/*Mandrillus* clade, *Procercocebus*. J. Hum. Evol. 53, 69–102.

Gilbert, C.C., 2013. Cladistic analysis of extant and fossil African papionins using craniodental data. J. Hum. Evol. 64, 399–433.

Gilbert, C.C., Goble, E.D., Kingston, J.D., Hill, A., 2011. Partial skeleton of *Theropithecus brumpti* (Primates, Cercopithecidae) from the Chemeron Formation of the Tugen Hills, Kenya. J. Hum. Evol. 61, 347–362.

Glaunès, J.A., Joshi, S., 2006. Template estimation from unlabeled point set data and surfaces for computational anatomy. In: Pennec, X., Joshi, S. (Eds.), Proceedings of the International Workshop on the Mathematical Foundations of Computational Anatomy. Copenhagen, pp. 29–39.

Gonzales, L.A., Benefit, B.R., McCrossin, M.L., Spoor, F., 2015. Cerebral complexity preceded enlarged brain size and reduced olfactory bulbs in Old World monkeys. Nat. Commun. 6, 7580.

Gunz, P., 2015. Computed tools for paleoneurology. In: Bruner, E. (Ed.), Human paleoneurology. Switzerland, Springer, pp. 39–55.

Gunz, P., Mitteroecker, P., Neubauer, S., Weber, G.W., Bookstein, F.L., 2009. Principles for the virtual reconstruction of hominin crania. J. Hum. Evol. 57, 48–62.

Heaton, J.L., 2006. Taxonomy of the Sterkfontein fossil Cercopithecinae: the Papionini of Members 2 and 4 (Gauteng, South Africa). Ph.D. Dissertation, Indiana University.

Hilgetag, C.C., Barbas, H., 2005. Developmental mechanics of the primate cerebral cortex. Anat. Embryol. 210, 411–417.

Holloway, R.L., 1978. The relevance of endocasts for studying primate brain evolution. In: Noback, C.R. (Ed.), Sensory Systems of Primates. New York, Plenum Press, pp. 181–200.

Holloway, R.L., Broadfield, D.C., Yuan, M.S., 2004. The Human Fossil Record: Brain Endocasts, the Paleoneurological Evidence. Wiley-Liss, New York.

Isler, K., Kirk, E.C., Miller, J.M.A., Albrecht, G.A., Gelvin, B.R., Martin, R.D., 2008. Endocranial volumes of primate species: scaling analyses using a comprehensive and reliable data set. J. Hum. Evol. 55, 967–978.

Jablonski, N.G., 1993. *Theropithecus*: The Rise and Fall of a Primate Genus. Cambridge University Press, Cambridge.

Jablonski, N.G., 2002. Fossil Old World monkeys: the late Neogene radiation. In: Hartwig, W.C. (Ed.), The Primate Fossil Record. Cambridge University Press, Cambridge, pp. 255–299.

Jablonski, N.G., Frost, S., 2010. Cercopithecoidea. In: Werdelin, L., Sanders, W.J. (Eds.), Cenozoic Mammals of Africa. University of California Press, Berkeley, pp. 393–428.

Jablonski, N.G., Leakey, M.G., 2008. Koobi Fora Research Project. Vol. 6. The Fossil Monkeys. California Academy of Sciences, San Francisco.

Jolly, C.J., 1972. The classification and natural history of *Theropithecus* (*Simopithecus*) (Andrews, 1916), baboons of the African Plio-Pleistocene. Bull. Br. Mus. Nat. Hist. Geol. 22, 1–122.

Kashima, M., Sawada, K., Fukunishi, K., Sakata-Haga, H., Tokado, H., Fukui, Y., 2008. Development of cerebral sulci and gyri in fetuses of cynomolgus monkeys (*Macaca fascicularis*). II. Gross observation of the medial surface. Brain Struct. Funct. 212, 513–520.

Kobayashi, Y., Matsui, T., Haizuka, Y., Ogihara, N., Hirai, N., Matsumura, G., 2014. Cerebral sulci and gyri observerd on macaque endocasts. In: Akazawa, T., Ogihara, N., Tanabe, H.C., Terashima, H. (Eds.), Dynamics of learning in Neanderthals and modern humans, Volume 2. Springer, Japan, pp 131–137.

Lê, S., Josse, J., Husson, F., 2008. FactoMineR: an R package for multivariate analysis. J. Stat. Softw. 25, 1–18.

Leakey, M.G., 1982. Extinct large colobines from the Plio-Pleistocene of Africa. Am. J. Phys. Anthropol. 58, 153–172.

Leakey, M.G., 1993. Evolution of *Theropithecus* in the Turkana Basin. In: Jablonski, N.G. (Ed.), *Theropithecus*: The Rise and Fall of a Primate Genus. Cambridge University Press, Cambridge, pp. 85–123.

Maier, W., 1970. New fossil Cercopithecoidea from the lower Pleistocene cave deposits of the Makapansgat Limeworks, South Africa. Palaeont. Afr. 13, 69–107.

Maier, W., 1972. The first complete skull of *Simopithecus darti* from Makapansgat, South Africa, and its systematic position. J. Hum. Evol. 1, 395–405.

Malkova, L., Heuer, E., Saunders, R.C., 2006. Longitudinal magnetic resonance imaging study of rhesus monkey brain development. Eur. J. Neurosci. 24, 3204–3212.

Martin, R.D., 1993. Allometric aspects of skull morphology in *Theropithecus*. In: Jablonski, N. (Ed.), *Theropithecus*: The Rise and Fall of a Primate Genus. Cambridge University Press, Cambridge, pp. 273–298.

McFadden, P.L., Brock, A., Partridge, T.C., 1979. Palaeomagnetism and the age of the Makapansgat hominid site. Earth Planet. Sci. Lett. 44, 373–382.

McKee, J.K., 1993. Taxonomic and evolutionary affinities of *Papio izodi* fossils from Taung and Sterkfontein. Palaeont. Afr. 30, 43–49.

McKee, J.K., Keyser, A.W., 1994. Craniodental remains of *Papio angusticeps* from the Haasgat cave site, South Africa. Int. J. Primatol. 15, 823–841.

McKee, J.K., Thackeray, J.F., Berger, L.R., 1995. Faunal assemblage seriation of Southern African Pliocene and Pleistocene fossil deposits. Am. J. Phys. Anthropol. 96, 235–250.

McKee, J.K., von Mayer, A., Kuykendall, K., 2011. New species of *Cercopithecoides* from Haasgat, North West Province, South Africa. J. Hum. Evol. 60, 83–93.

Mitteroecker, P., Bookstein, F.L., 2011. Linear discrimination, ordination, and the visualization of selection gradients in modern morphometrics. Evol. Biol. 38, 100–114.

Neubauer, S., 2014. Endocasts: possibilities and limitations for the interpretation of human brain evolution. Brain Behav. Evol. 84, 117–134.

Neubauer, S., Gunz, P., Hublin, J.-J., 2009. The pattern of endocranial ontogenetic shape changes in humans. J. Anat. 215, 240–255.

Neubauer, S., Gunz, P., Hublin, J.-J., 2010. Endocranial shape changes during growth in chimpanzees and humans: a morphometric analysis of unique and shared aspects. J. Hum. Evol. 59, 555–566.

Pillay, P., Manger, P.R., 2007. Order-specific quantitative patterns of cortical gyrification. Eur. J. Neurosci. 25, 2705–2712.

Radinsky, L., 1974. The fossil evidence of anthropoid brain evolution. Am. J. Phys. Anthropol. 41, 15–28.

Rakic, P., 1995. A small step for the cell, a giant leap for mankind: a hypothesis of neocortical expansion during evolution. Trends Neurosci 18, 383–388.

Sawada, K., Sun, X.Z., Fukunishi, K., Kashima, M., Sakata-Haga, H., Tokado, H., Aoki, I., Fukui, Y., 2009. Developments of sulcal pattern and subcortical structures of the forebrain in cynomolgus monkey fetuses: 7-tesla magnetic resonance imaging provides high reproducibility of gross structural changes. Brain Struct. Funct. 213, 469–480.

Scott, J.E., 2011. Folivory, frugivory, and postcanine size in the Cercopithecoidea revisited. Am. J. Phys. Anthropol. 146, 20–27.

Smith, B.H., 1991. Dental development and the evolution of life history in Hominidae. Am. J. Phys. Anthropol. 86, 157–174.

Smith, R.J., Jungers, W.L., 1997. Body mass in comparative primatology. J. Hum. Evol. 32, 523–559.

Specht, M., Lebrun, R., Zollikofer, C.P.E., 2007. Visualizing shape transformation between chimpanzee and human braincases. Vis. Comput. 23, 743–751.

Subsol, G., 1995. Construction automatique d'atlas anatomiques morphométriques à partir d'images médicales tridimensionnelles. Ph.D. Dissertation, École Centrale de Paris.

Subsol, G., 1998. Crest lines for curve based warping. In: Toga, A. (Ed.), Brain Warping. Academic Press, San Diego, pp. 241–262.

Subsol, G., Gesquière, G., Braga, J., Thackeray, F., 2010. 3D automatic methods to segment "virtual" endocasts: state of the art and future directions. Am. J. Phys. Anthropol. 141 (Suppl. 50), 226–227.

Swindler, D.R., Beynon, A.D., 1993. The development and microstructure of the dentition of *Theropithecus*. In: Jablonski, N. (Ed.), *Theropithecus*: The Rise and Fall of a Primate Genus. Cambridge University Press, Cambridge, pp. 351–381.

Szalay, F.S., Delson, E., 1979. Evolutionary History of the Primates. Academic Press, New York.

Tallinen, T., Chung, J.Y., Rousseau, F., Girard, N., Lefèvre, J., Mahadevan, L., 2016. On the growth and form of cortical convolutions. Nat. Physics, DOI: 10.1038/nphys3632.

Toro, R., 2012 On the possible shapes of the brain. Evol. Biol. 39, 600–612.

Toro, R., Burnod, Y., 2005. A morphogenetic model for the development of cortical convolutions. Cereb. Cortex 15, 1900–1913.

Van Essen, D.C., 1997. A tension-based theory of morphogenesis and compact wiring in the central nervous system. Nature 385, 313–318

Weber, G.W., Bookstein, F.L., 2011. Virtual Anthropology: a guide to a new interdisciplinary field. Springer, London.

Welker, W., 1990. Why does cerebral cortex fissure and fold? A review of determinants of gyri and sulci. In: Jones, E.G., Peters, A. (Eds.), Comparative structure and evolution of cerebral cortex, Part II, vol 8B. Plenum, New York, pp. 3–136.

Yoshizawa, S., Belyaev, A., Yokota, H., Seidel, H.-P., 2007. Fast and faithful geometric algorithm for detecting crest lines on meshes. Proceedings of the 15th Pacific Conference on Computer Graphics and Applications, pp. 231–237.

Yoshizawa, S., Belyaev, A.,Yokota, H., Seidel, H.P., 2008. Fast, robust, and faithful methods for detecting crest lines on meshes. Computer Aided Geom. D. 25, 545–560.

Zollikofer, C.P.E., 2002. A computational approach to paleoanthropology. Evol. Anthropol. 11, 64–67.

Zollikofer, C.P.E., Ponce De León, M.S., Martin, R.D., 1998. Computer-assisted paleoanthropology. Evol. Anthropol. 6, 41–54.

Zollikofer, C.P.E., Ponce De León, M.S., Martin, R.D., 1998. Computer-assisted paleoanthropology. Evol. Anthropol. 6, 41–54.

Figure legends

Figure 1. Successive processing steps in the deformation-based shape comparisons. First, the surfaces are rigidly aligned in position, orientation, and scale with respect to a reference surface (A). From an initial set of aligned surfaces and an ellipsoidal template (B), the deformation fields, the global mean shape, and the registered surfaces are computed (C) and the taxon mean shapes are generated (D). The global mean shape (GMS) is subsequently deformed to the fossil specimens (E). The distances from the GMS to the specimens are rendered by color maps and vectors (F). In C and E, the arrows represent the deformations from the GMS to individuals. N indicates the maximum number of specimens included in the sample. For each view, the hidden side of the endocranial surface was virtually removed.

Figure 2. Log endocranial volume (ECV) against log body mass for Plio-Pleistocene and extant cercopithecoid specimens. For specimens for which sex is not known (i.e., one *Chlorocebus aethiops*, one *Colobus guereza*, one *Cercocebus atys*, one *Mandrillus leucophaeus,* plus the *Cercopithecoides williamsi* neurocranium MP 36), both the male (higher) and the female (lower) body masses are plotted and the corresponding symbols linked by dotted lines.

Figure 3. Between-group principal component analysis (bgPCA) of the deformation-based shape comparisons of the endocasts extracted from Plio-Pleistocene and extant cercopithecoid specimens.

Figure 4**.** Comparative maps of morphological deformations from the global mean shape computed for the extant cercopithecoid sample (GMS) to specimens of *Pp*. *jonesi*, *Pp*. *broomi*, *Pp*. *whitei*, *Pp*. *antiquus*, *Pp*. sp., and *P*. *izodi*. Endocasts are shown in superior (sup),

anterior (ant), and lateral (lat) right (r) views. Cumulative displacement variations are rendered by a pseudo-color scale ranging from dark blue (lowest values) to red (highest values) at the fossil individual surfaces. The vectors represent both the magnitude and orientation of the deformations from the GMS to the fossil specimens. The maximum value of the color bar (3 mm) is considered to be the most appropriate compromise representation of both global and local deformations, even if some recorded deformations exceeded this value. For each view, the hidden side of the endocranial surface was virtually removed.

Figure 5**.** Comparative maps of morphological deformations from the global mean shape computed for the extant cercopithecoid sample (GMS) to specimens of *T*. *o*. *oswaldi*, *T*. *o*. *darti*, *C*. *williamsi*, and an undetermined taxon. Endocasts are shown in superior (sup), anterior (ant), and lateral (lat) right (r) views. Cumulative displacement variations are rendered by a pseudo-color scale ranging from dark blue (lowest values) to red (highest values) at the fossil individual surfaces. The vectors represent both the magnitude and orientation of the deformations from the GMS to the fossil specimens. The maximum value of the color bar (3 mm) is considered to be the most appropriate compromise representation of both global and local deformations, even if some recorded deformations exceeded this value. For each view, the hidden side of the endocranial surface was virtually removed.

Figure 6. Hierarchical classification based on the distances computed from the endocast deformation (GMS to individuals) extracted from Plio-Pleistocene and extant cercopithecoid specimens. The genus sampled at each terminal branch is coded by a number. The common branch is not represented here. Papionini: groups A to G; Colobini: groups H and I; Cercopithecini: groups J to L.

Figure 7. Virtual reconstructions of *Parapapio* endocasts with sulcal impressions in superior (sup), lateral (lat) right (r), and left (l) views (arc = sulcus arcuatus, ip = sulcus intraparietalis, l = sulcus lunatus, lc = sulcus calcarinus lateralis, oci = sulcus occipitalis inferior, p = sulcus principalis, s = sulcus lateralis, ts = sulcus temporalis superior, sca = sulcus subcentralis anterior, scp = sulcus subcentralis posterior). Only sulci mentioned in the text are labeled. Question marks indicate uncertain sulcal identifications. Images not to scale.

Figure 8. Virtual reconstructions of *Theropithecus* and *Cercopithecoides* endocasts along with that of the undetermined specimen STS 538, with sulcal impressions in superior (sup), lateral (lat) right (r), and left (l) views (arc = sulcus arcuatus, ip = sulcus intraparietalis, l = sulcus lunatus, lc = sulcus calcarinus lateralis, oci = sulcus occipitalis inferior, p = sulcus principalis, s = sulcus lateralis, ts = sulcus temporalis superior, sca = sulcus subcentralis anterior, and scp = sulcus subcentralis posterior). Only sulci mentioned in the text are labeled. Question marks indicate uncertain sulcal identifications. Images not to scale.

Table 1

List of the Plio-Pleistocene and extant cercopithecoid specimens/samples included in the study.

	Specimen/ sample	Site/ provenance[a]	Source	Stored at[b]	µCT equipment[c]	µCT acquisition voxel size (µm)
|Fossil taxa						
Parapapio jonesi	STS 565	Sterkfontein (Member 4)	Freedman, 1957; Eisenhart, 1974; Brain, 1981; Jablonski, 2002	Ditsong	Necsa	71.9
Parapapio broomi	MP 224[d], STS 564	Sterkfontein (Member 4) Makapansgat (Member 4)	Freedman, 1957, 1976; Brain, 1981; McKee, 1993; Jablonski, 2002; Heaton, 2006	Ditsong Wits	Necsa Pal. Centre	71.9–81.6
Parapapio whitei	MP 221[d]	Makapansgat (Member 4)	Freedman, 1976; Gilbert, 2013	Ditsong Wits	Necsa Pal. Centre	71.2
Parapapio antiquus	TP 8	Taung	Freedman, 1957, 1961	Wits	Pal. Centre	80.0
Parapapio sp.	M 3133[d]	Makapansgat (Member 4)	Fourie et al., 2008	Wits	Pal. Centre	78.7
Papio izodi	TP 7	Taung	Freedman, 1957, 1961; Jablonski and Frost, 2010	Wits	Pal. Centre	76.9
Theropithecus oswaldi oswaldi	SK 561	Swartkrans (Member 1)	Freedman, 1957; Freedman and Brain, 1977; Brain, 1981; Jablonski, 2002	Ditsong	Necsa	99.9
Theropithecus oswaldi	M 3073, MP	Makapansgat	Maier, 1972 ; Freedman,	Wits	Pal. Centre	71.2

darti	222	(Member 4)	1976 ; Jablonski, 1993, 2002; Jablonski and Frost, 2010			
Cercopithecoides williamsi	M 3055, MP 3a/M 203/AD 1326-3, MP 36/M 236/AD 1326-6	Makapansgat (Member 4)	Mollett, 1947; Freedman, 1957; Maier, 1970; Eisenhart, 1974; Jablonski, 2002; Heaton, 2006; Fourie et al., 2008	Wits	Pal. Centre	71.2–78.8
Undetermined	STS 538	Sterkfontein (Member 4)	Brain, 1981; Heaton, 2006	Ditsong	Necsa	56.2
Extant taxa						
Papio (*anubis n* = 2, *cynocephalus n* = 1, *cynocephalus kindae n* = 2, *hamadryas n* = 1, *ursinus n* = 2)	*n* = 8	Central Africa, Congo, Ethiopia		MNHN MRAC	AST-RX FERMaT	32.7–122.9
Theropithecus gelada	*n* = 3	Ethiopia		MNHN AMNH	AST-RX MIF	35.0–95.8
Lophocebus albigena	*n* = 4	Cameroon, Congo, Gabon		MNHN MRAC	AST-RX FERMaT	32.7–66.2
Mandrillus (*leucophaeus n* = 3, *sphinx n* = 3)	*n* = 6	Cameroon, Guinea, unknown provenance		MRAC MHNT AMNH	FERMaT MIF CBCT	32.7–200.0
Cercocebus (*atys n* = 2, *torquatus n* = 1)	*n* = 3	Cameroon, Liberia		MRAC	FERMaT	32.7
Macaca (*mulatta n* = 1, *sylvanus n* = 1, sp. *n* =	*n* = 3	India, unknown provenance		MHNT	FERMaT	32.7

1)

Cercopithecus cephus	*n* = 2	Congo, Guinea	MHNT	FERMaT MEDES	32.7
Erythrocebus patas	*n* = 2	Congo, Senegal	MHNT MRAC	FERMaT	32.7
Cholorocebus (*aethiops n* = 3, *pygerythrus n* = 2)	*n* = 5	Congo, Republic of Cabo Verde, Senegal, South Africa	MRAC MHNT	FERMaT	32.6–32.7
Colobus (*angolensis n* = 1, *guereza n* = 8)	*n* = 9	Congo, Ethiopia, unknown provenance	MNHN MRAC AMNH MHNT	AST-RX FERMaT MIF	32.7–35.0
Piliocolobus foai	*n* = 1	Congo	MRAC	FERMaT	32.7

[a] Unless mentioned, the specimens from Sterkfontein and Swartkrans derive from Member 4 and Member 1, respectively, and those from Makapansgat are from Member 4 (Brain, 1981; Heaton, 2006).

[b] Abbreviations for storage locations: Ditsong = Ditsong National Museum of Natural History, Pretoria; Wits = University of the Witwatersrand, Johannesburg; MNHN = Muséum national d'Histoire naturelle, Paris; MRAC = Musée royal de l'Afrique centrale, Tervuren; AMNH = American Museum of Natural History, New York; MHNT = Museum d'Histoire naturelle de Toulouse

[c] Nesca = South African Nuclear Energy Corporation, Pretoria (Hoffman and De Beer, 2012); Pal. Centre = Palaeosciences Centre, University of the Witwatersrand, Johannesburg; AST-RX = Accès Scientifique à la Tomographie à Rayons-X, MNHN, Paris; FERMaT = Fédération Fluides Energie Réacteurs Matériaux et Transferts, Toulouse; MIF = Microscopy and Imaging Facility, AMNH, New York (data provided by Pr Eric Delson and the AMNH Department of Mammalogy, some specimens were downloaded from www.morphosource.org, Duke University), MEDES = Faculté de Chirurgie Dentaire de Toulouse.

[d] Uncertain stratigraphic localization, but an attribution to Member 4 is proposed by the catalog of the University of the Witwatersrand for M 3133, and the descriptions of MP 221 and MP 224 by Freedman (1976) suggest an origin in Member 4.

Table 2

Endocranial volumes (ECV) assessed (in cm^3) in Plio-Pleistocene and extant cercopithecoid specimens/samples.

Specimen/sample		ECV (cm^3)
Fossil taxa		
Pp. jonesi	STS 565	114
Pp. broomi	MP 224	160
	STS 564	165
	Mean	162
Pp. whitei	MP 221	150
Pp. antiquus	TP 8	133
P. izodi	TP 7	118
T. o. oswaldi	SK 561	168
T. o. darti	M 3073	170
	MP 222	134
	Mean	152
C. williamsi	M 3055	128
	MP 3	174
	MP 36	165
	Mean	156
Extant taxa		
Papio (*n* = 8)	Mean	171
	Range	131–204
Theropithecus (*n* = 2)	Mean	146
	Range	114–179
Lophocebus (*n* = 4)	Mean	101
	Range	92–117
Mandrillus (*n* = 5)	Mean	151
	Range	129–177
Cercocebus (*n* = 3)	Mean	99
	Range	91–105
Macaca (*n* = 2)	Mean	9
	Range	78–107
Cercopithecus (*n* = 2)	Mean	61

	Range	52–70
Erythrocebus (*n* = 2)	Mean	79
	Range	54–103
Chlorocebus (*n* = 5)	Mean	70
	Range	64–74
Colobus (*n* = 5)	Mean	86
	Range	73–91
Piliocolobus (*n* = 1)		70

Figure_1
Click here to download high resolution image

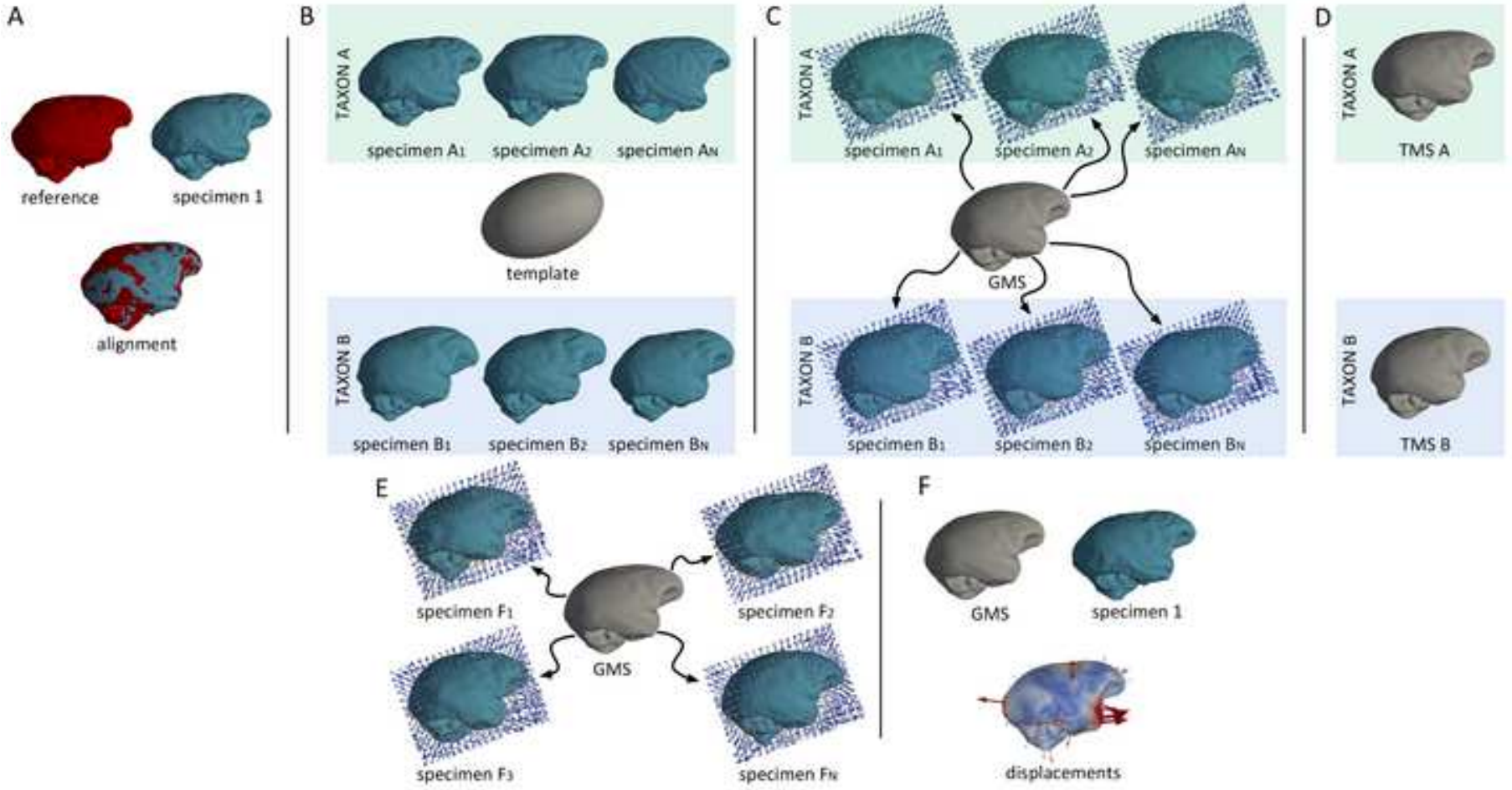

Figure_2
Click here to download high resolution image

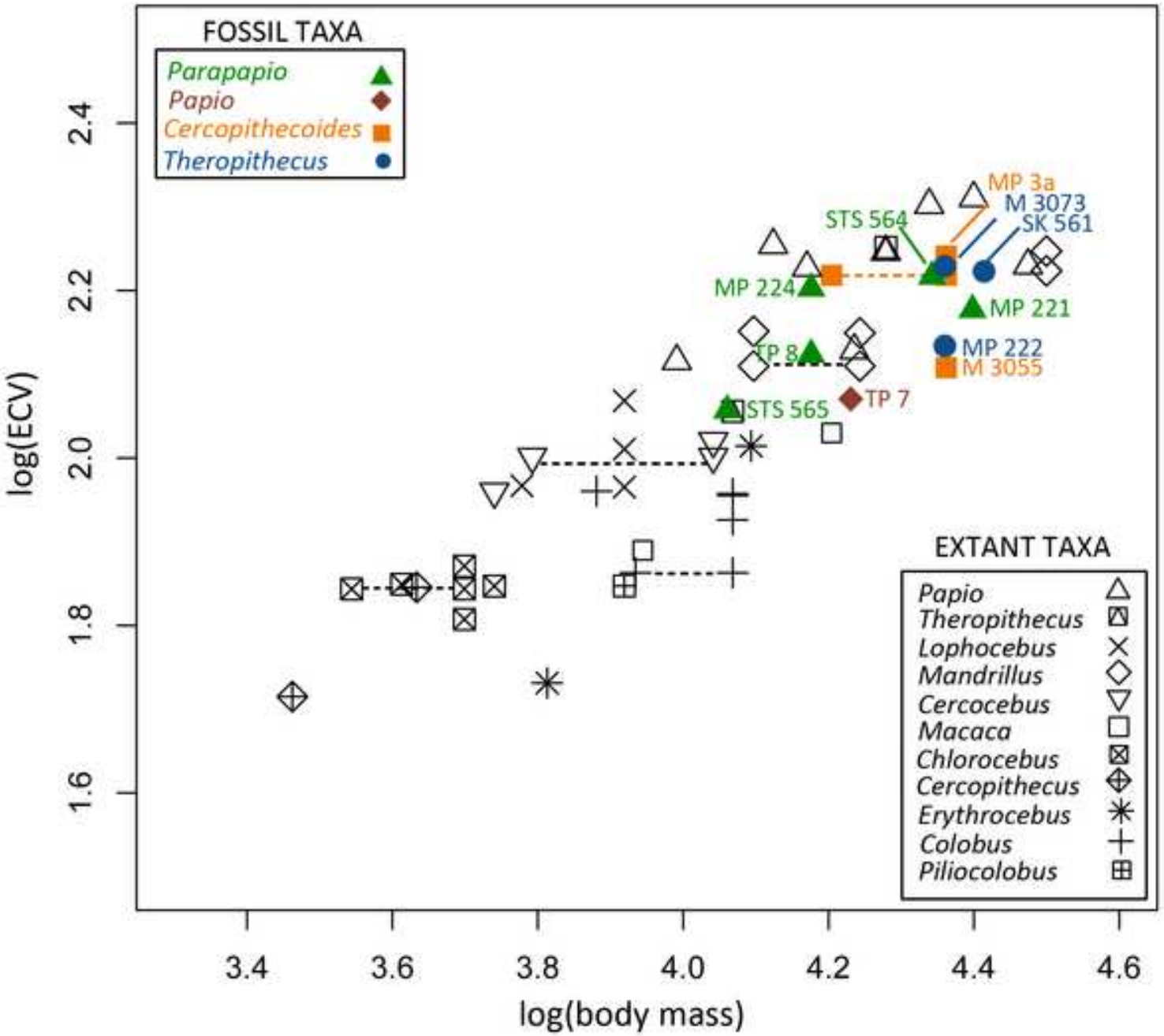

Figure_3
Click here to download high resolution image

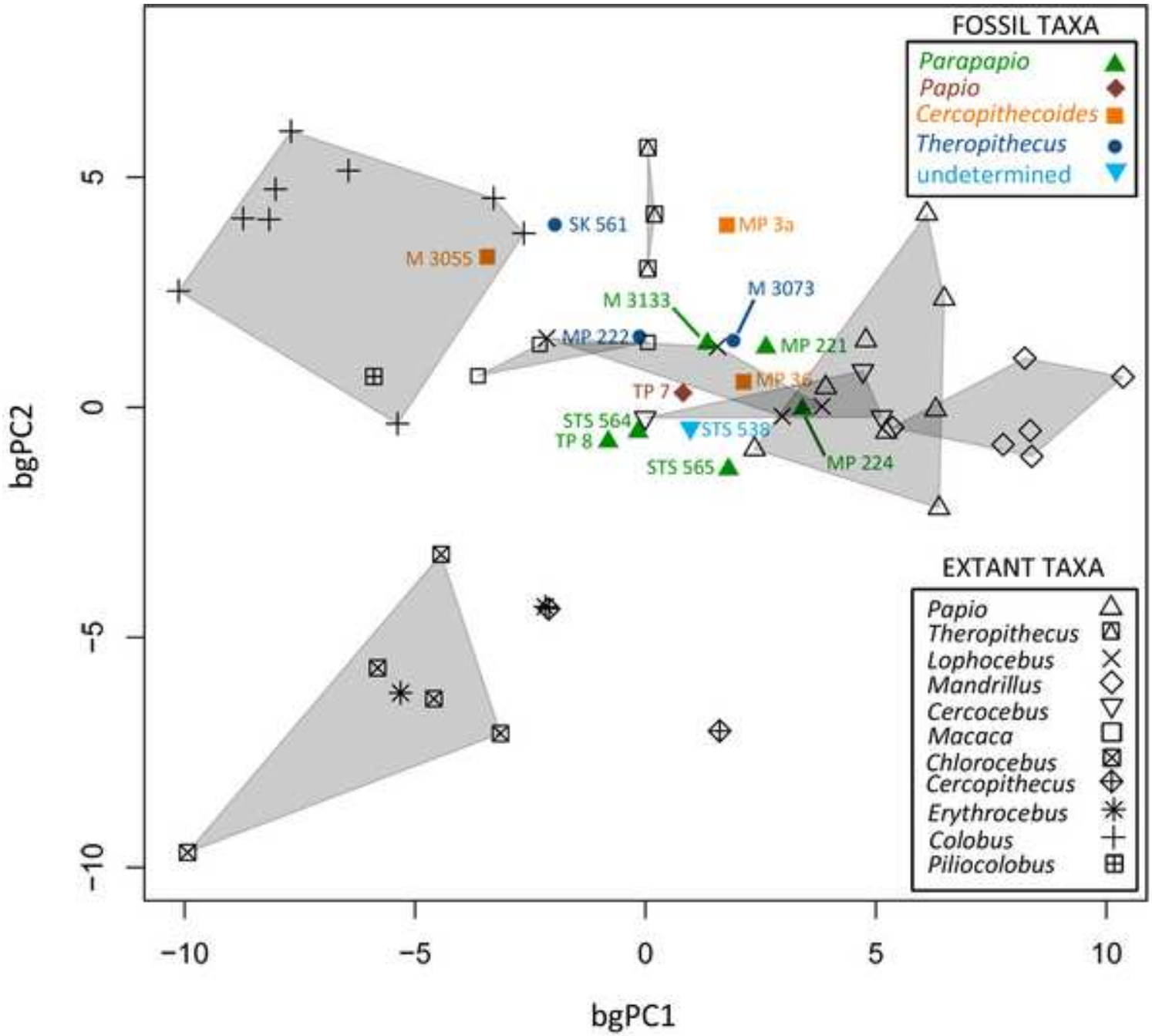

Figure_4
Click here to download high resolution image

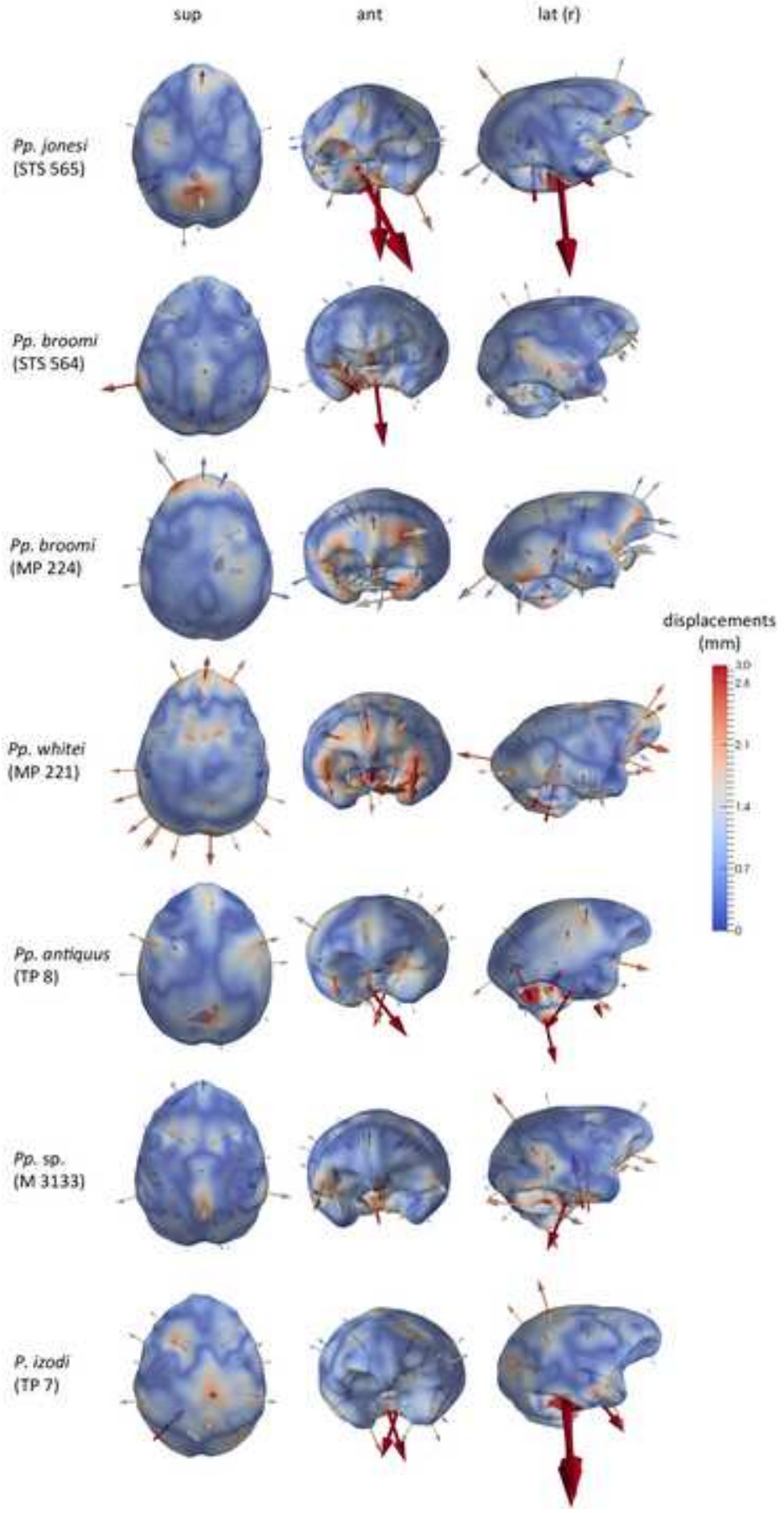

Figure_5
Click here to download high resolution image

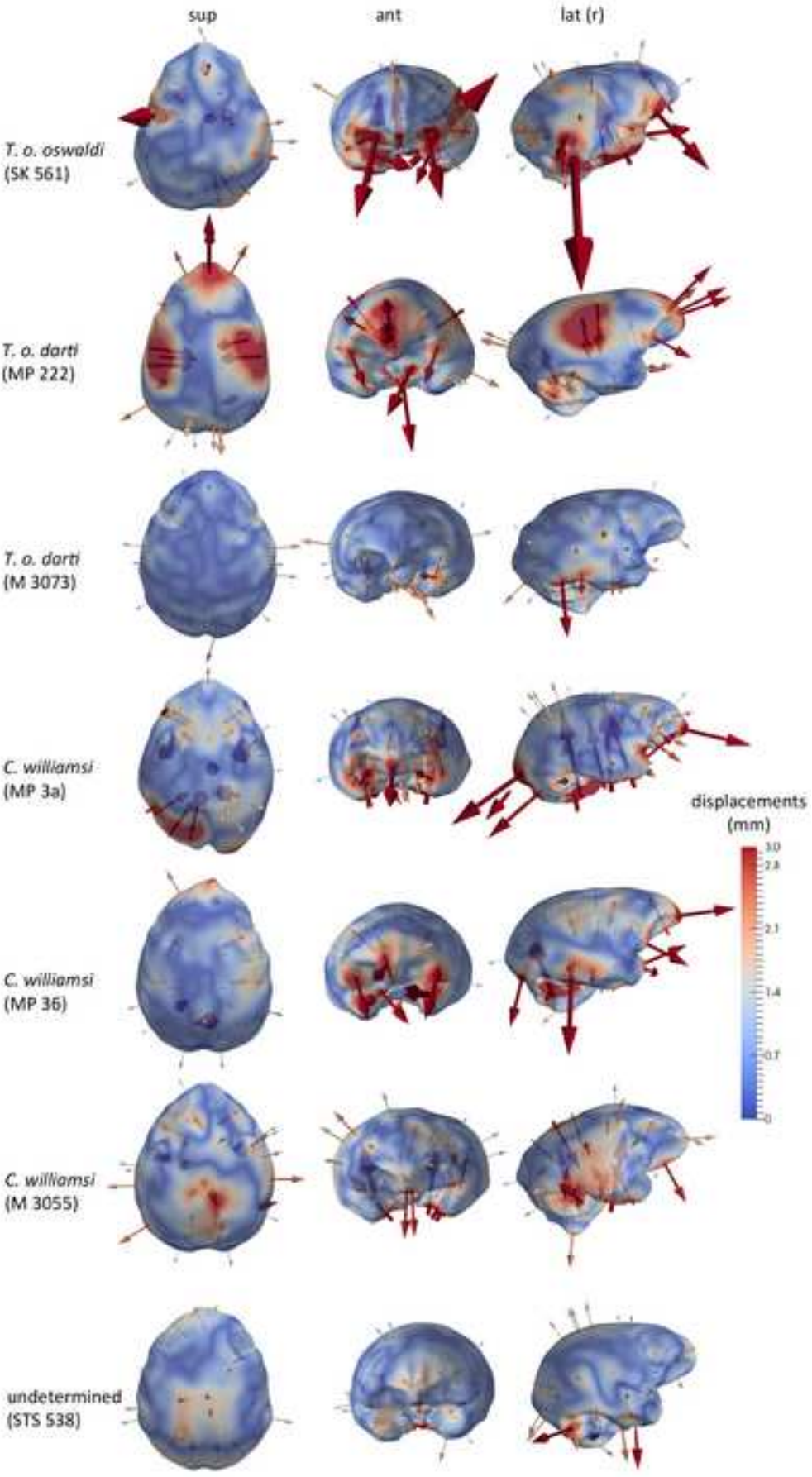

Figure_6
Click here to download high resolution image

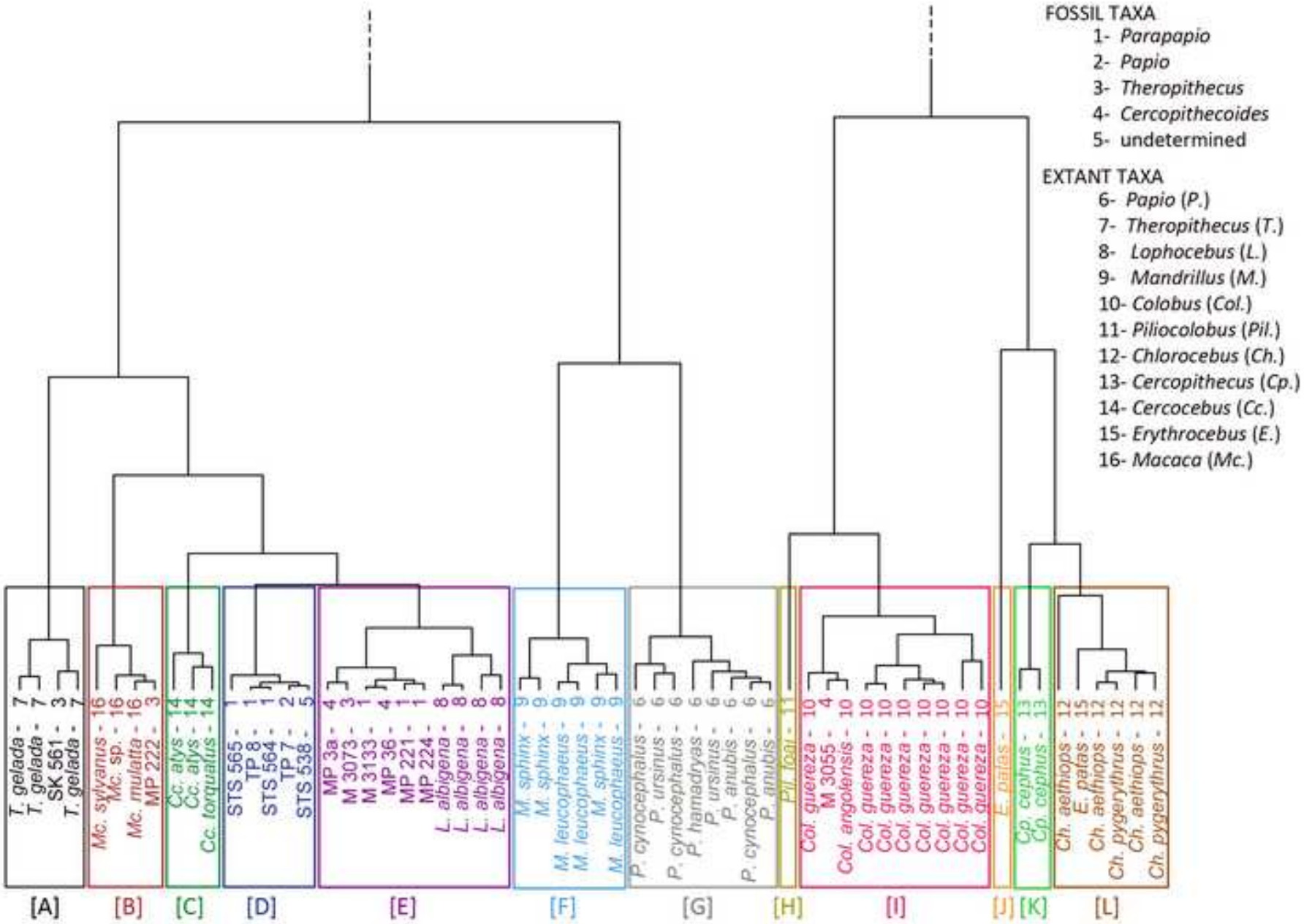

Figure_7
Click here to download high resolution image

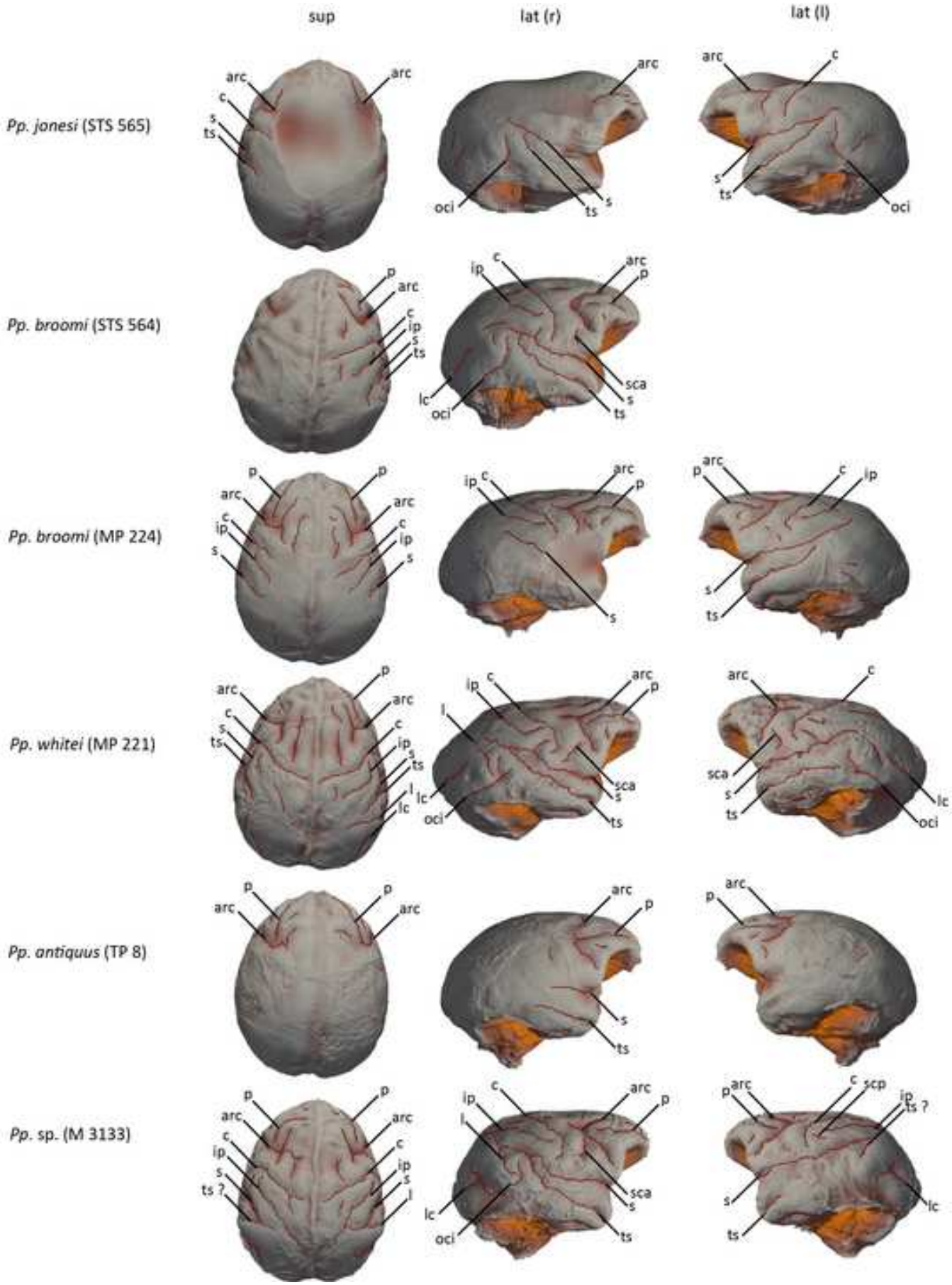

Figure_8
Click here to download high resolution image